Hydrol. Earth Syst. Sci., 30, 1675–1689, 2026
https://doi.org/10.5194/hess-30-1675-2026

Hydrology and Earth System Sciences
Open Access
EGU

Elucidating loessal landslide initiation in wood- and shrub-land by hydro-mechanical heterogeneity

Ruijie Yang, Chao Ma, Xi Yang, Yan Zhang, Liqun Lyu, and Xinying Wang

School of Soil and Water Conservation, Beijing Forestry University, Beijing 100083, PR China

Correspondence: Chao Ma (sanguoxumei@163.com)

Received: 7 December 2025 – Discussion started: 23 December 2025
Revised: 9 March 2026 – Accepted: 10 March 2026 – Published: 30 March 2026

Abstract. Vegetation recovery on the Chinese Loess Plateau has markedly changed the hydrological and mechanical controls on hillslope erosion, shifting sediment production from runoff-driven erosion to gravity-driven processes such as rainfall-induced loessal landslides. Presently, few studies have clearly documented the differences in landslide erosion and initiation between shrubland and woodland. We conducted field investigations, rainfall soil-moisture observations, dye-tracer experiments, and soil-root tests, to examine landslide characteristics in terms of geometry and volume, excess soil-water ratio, preferential-flow pathways, and failure potential in the two stands. Rainfall-induced loessal landslides in the shrubland stand have shallower failure depths and smaller volumes but are wider than those in the woodland stand, and they are triggered under lower contributing area-slope conditions. Moreover, vertical infiltration in the woodland stand tends to be more stable and efficient, characterized by greater water penetration depth and enhanced pore connectivity. The relationship between the excess soil-water ratio and soil-water storage demonstrates that subsurface flow in woodland stand is triggered at relatively lower degrees of saturation. This behavior is attributed to well-developed preferential-flow pathways and reduced matric suction. The landscape dissection-rainfall index indicates lower landslide susceptibility on steep woodland slopes than on steep shrubland slopes, consistent with the lower landslide density in woodland relative to shrubland. Overall, these hydrological and mechanical contrasts indicate that woodland slopes, by combining deep root systems, stable preferential-flow pathways, and strong mechanical reinforcement, support an effective subsurface flow system that enhances infiltration and delays shallow saturation, thus improving slope stability. These results highlight the need to reassess sediment production on the Loess Plateau by explicitly accounting for landslides rather than attributing it solely to runoff-driven erosion.

1 Introduction

The Chinese Loess Plateau is one of the most erosive landscapes in the world (Fu et al., 2016; Borrelli et al., 2020; Bai et al., 2024). Since 1980, ecological rehabilitation has significantly improved regional vegetation cover and structure, with vegetation cover now reaching approximately 60 % (Feng et al., 2016; Deng et al., 2022; Liao et al., 2025). Restored vegetation, optimized plant community structure, and surface litter accumulation have enhanced water storage capacity and slope stability (Yan et al., 2024; Liu et al., 2025). Since 2010, the region has experienced several rainstorms that are unprecedented in the historical record, as exemplified by storms in 2013, 2017, and 2025 (Tang et al., 2020; Deng et al., 2022; Yang et al., 2023; Hao et al., 2024). Subsequent studies have reported a shift in the dominant erosion process from dispersed runoff erosion to gravitational mass movements (Yang et al., 2024; Du et al., 2025). These findings sufficiently indicate that vegetation recovery on Chinese Loess Plateau alters the dominant sediment-producing processes and soil-erosion patterns.

Vegetation recovery can enhance ecosystem functioning and alter the rainwater infiltration pathways (Gu et al., 2019; Wang et al., 2022; Guan et al., 2024). Increases in surface cover and root penetration significantly enhance rainfall infiltration and promote greater spatial heterogeneity, non-uniform infiltration patterns, and preferential-flow pathways (Li et al., 2007; Zhao et al., 2022). Preferential flow often

serves as a primary pathway for rainfall infiltration and can bypass soil-matrix pores to reach deeper soil layers (Bachmair et al., 2012; Franklin et al., 2021). Preferential flow intensity and morphology vary markedly among vegetation types. Woodland slopes are characterized by deep, continuous macropore channels, predominantly vertical preferential flow, rapid infiltration, and greater deep-soil water storage (Niu et al., 2023; Cai et al., 2024; Zhang et al., 2025). Shrubland slopes exhibit predominantly lateral and diffuse subsurface flow with weak vertical components, thereby retaining much of the infiltrating water in shallow soil layers (Wang et al., 2020; An et al., 2022; Liang et al., 2023; Zhang et al., 2024). Herbaceous slopes rely mainly on surface cracks and earthworm burrows to route water, and therefore preferential flow channels are sparse and discontinuous (Wen et al., 2020; Niu et al., 2023; Li et al., 2025). Vegetation recovery has significantly restructured the soil bio-pore system through root penetration, thereby facilitating the development of preferential-flow pathways and making infiltration regimes more heterogeneous (Zhao et al., 2022; Guan et al., 2024). However, preferential-flow infiltration on steep slopes, particularly at landslide sites with different vegetation types, has not been adequately investigated. During heavy storms, preferential flow can regulate spatiotemporal subsurface water dynamics and act as a biologically mediated control on slope stability.

Root morphology and spatial configuration influence rainwater infiltration pathways and soil-moisture redistribution (Fan et al., 2020; Li et al., 2023). On the Chinese Loess Plateau, two predominant vegetation types are recognized: woodlands dominated by *Robinia pseudoacacia* and *Pinus tabulaeformis*, and shrublands dominated by *Rosa xanthina* and *Hippophae rhamnoides*. Woodland trees typically develop deeply penetrating root systems, forming continuous macropore networks and vertical preferential-flow pathways (Zhao et al., 2022; Cai et al., 2024; Wang and Zhang, 2024). These structures facilitate rapid rainfall infiltration into deep soil layers, enhance subsurface moisture retention, delay surface saturation, and reduce surface runoff (Souza et al., 2023; Cai et al., 2024; Hu et al., 2025). In contrast, shrubs develop a dense, fibrous root matrix that promotes mesopores and capillaries formation, thereby accelerating the formation of subsurface saturation zones and limiting vertical percolation (Laycock, 1967; Souza et al., 2023; Xiao et al., 2024; Yamase et al., 2024). Therefore, plant roots can control preferential-flow patterns and alter hillslope hydrology. However, few studies have examined how the hydrological effects of mature vegetation influence landslides on the Chinese Loess Plateau.

To examine the hydrological and mechanical heterogeneity in mature woodland and shrubland stands on steep slopes and its implications for slope stability, we first analyze landslide geometry and landscape dissection for slides triggered by a low-intensity storm from 3 to 6 October 2021. Then, we assess hydrological heterogeneity in mature woodland and shrubland using soil-moisture observations, excess soil-water ratios across different soil-water storage levels, and preferential-flow pathway identification. Mechanical heterogeneity is characterized by soil and root strength parameters, the soil water characteristic curve (SWCC), and the hydraulic conductivity function (HCF). Finally, we evaluate slope failure potential in relation to landslide density in the two stands. This study mainly addresses the role of vegetation in modulating slope stability by analyzing real landslide cases. Our findings highlight the dual role of vegetation in mitigating landslide erosion and provide new insights into its nuanced effects on hillslope stability.

2 Research background

Study area

The study area lies in a forested catchment on the southeastern Loess Plateau in China (Fig. 1a). It is located in the downstream reach of the Caijiachuan watershed in Jixian County, Shanxi Province (Fig. 1b). The soil has an unconsolidated, porous structure. On steep slopes, woodland is dominated by *Robinia pseudoacacia* and shrubland by *Rosa xanthina*. Since the farmland reforestation policy was implemented in 1980, forest cover has recovered to about 70 %. During 1990–1995 and 1999–2002, the Mountain Improvement Technology Training Project enhanced forest regeneration. Currently, the local soil and water conservation measures serve as a benchmark within the Loess Plateau region. The area has four distincitive seasons and a cold semi-arid climate. The annual precipitation is approximately 579.1 mm, and the mean annual temperature is 9.9 °C. Most rain events occurs from June to September, accounting for more than 70 % of the annual precipitation. Prior to the 2021 event, a short-duration storm on 25–26 August 2003 triggered 18 landslides, with antecedent precipitation of 71.7 mm over 18 h and an intense 3 h rainfall of 24.4 mm (Wang et al., 2024). In contrast, the 2021 rainfall event was a low-intensity storm with prolonged antecedent precipitation of 121.8 mm over 72 h and a 6 h peak rainfall of 32.2 mm (Fig. 2). After the storm, post-storm documentation mainly focused on differences in landslide numbers, densities, slope aspects, and morphological metrics (Tang et al., 2023), while giving little attention to the hydrological and mechanical conditions of landslides in the two forested land types.

3 Materials and methods

3.1 Landslide information interpretation

To obtain landslide inventories for the woodland and shrubland, we acquired high-resolution orthoimages and digital elevation models (DEMs) using an unmanned aerial vehicle (UAV; DJI Inspire 2). Two systematic UAV flights

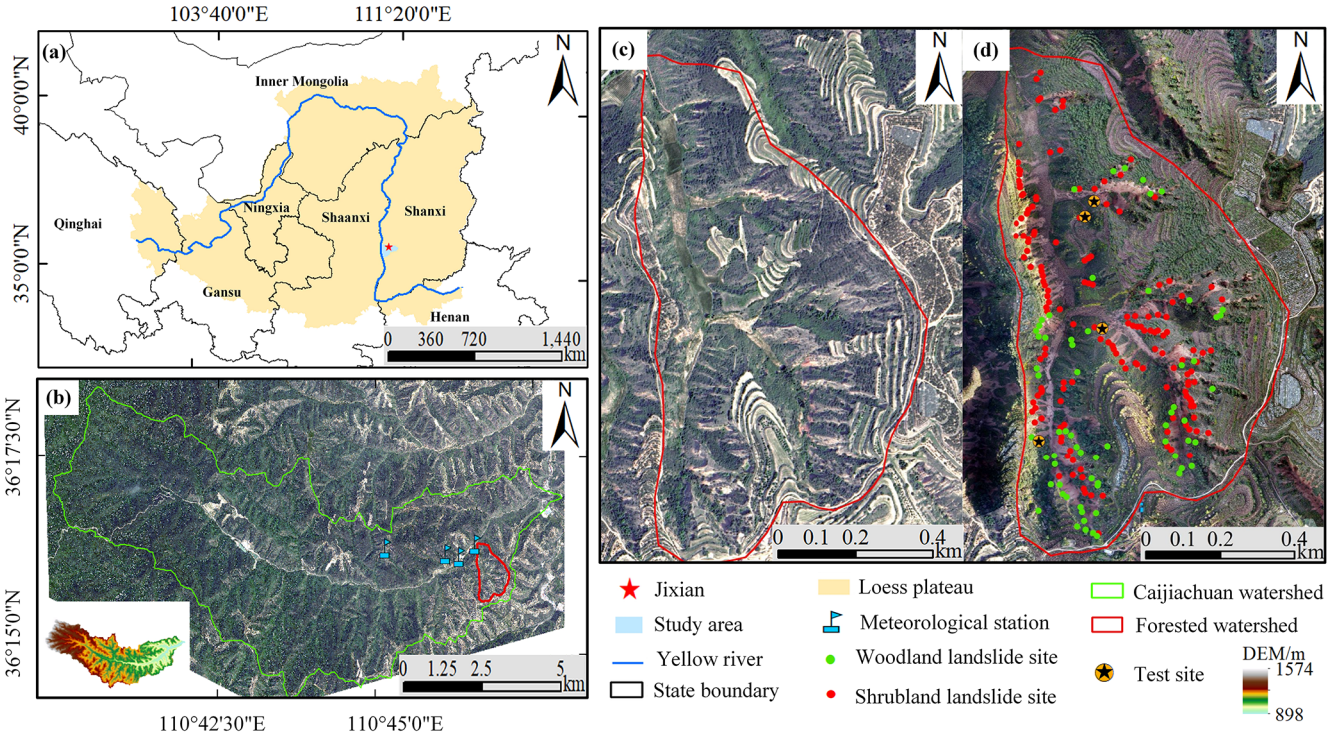

Figure 1. Geographical setting of the study area, with the **(a)** location of Caijiachuan watershed in the Loess Plateau, China, **(b)** the forested catchment and meteorological stations in downstream reach of Caijiachuan watershed, **(c)** 0.15 m resolution orthoimage on 12 October 2019, and **(d)** 0.10 m resolution orthoimage on 14 October 2021 showing the sites for soil-moisture observations and dye-tracer experiments.

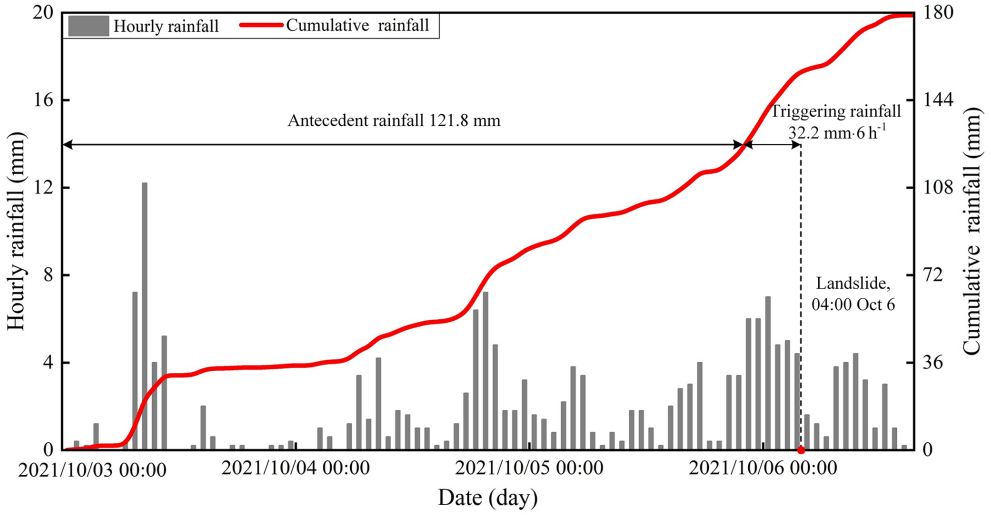

Figure 2. Hourly and cumulative rainfall from 3 to 6 October 2021.

with consistent flight and image overlap settings were conducted on 12 October 2019 (Fig. 1c) and 14 October 2021 (Fig. 1d). Pix4Dmapper (version 4.6, Pix4D SA, Switzerland) was used to generate ortho-mosaics and DEMs. These DEMs have spatial resolutions of 0.15 and 0.10 m, respectively, thereby supporting accurate landslide mapping. The landslide depths in the woodland and shrubland were measured during field investigations. Landslide point and areal densities are calculated by dividing the total number of landslides and the total scar area by the woodland and shrubland areas, respectively. The lateral extent of each landslide is the sum of the sidewall and head scarp areas. The unit upslope contributing area is the ratio of the total contributing area to the scar width. Slope gradients and associated unit contribut-

ing areas are computed from the DEM generated on 14 October 2021.

3.2 Rainfall, soil-moisture monitoring and sample collection

In the study area, the woodland has an open structure due to sparse-to-moderate tree density and high canopy height (Fig. 3a), whereas the shrubland has a closed structure because of high density and low canopy height (Fig. 3b). Each study site is dominated by single woody species, with *Robinia pseudoacacia* in the woodland and *Rosa xanthina* in the shrubland. Both land types have a well-developed herbaceous layer. To investigate the hillslope hydrology, we used frequency-domain reflectometry (FDR) soil-moisture sensors installed at depths of 30, 60, and 90 cm to record volumetric water content from May to August 2023 (Fig. 3c). A meteorological station at Caijiachuan Forest Station is approximately 2 km to the northwest of the study area. During soil-moisture sensor installation, we collected undisturbed soil samples near the FDR sensor locations. Bulk density, porosity, effective cohesion, internal friction angle, and unsaturated hydraulic properties were determined using an electronic balance, an oven, a GDS triaxial apparatus, and transient release and imbibition tests (Lu and Godt, 2013). Plant roots were collected to determine depth-dependent root distribution (Fig. 3d), root diameter, root area ratio, and tensile strength (Nimmo et al., 2009).

3.3 Excessive soil water due to preferential flow

Previous studies of preferential flow on the Loess Plateau have shown that continuous channels in woodland enhance deep soil water storage, whereas lateral and dispersed channels in shrubland keep water in shallow soil layers (Wang et al., 2019; An et al., 2022). Therefore, differences in preferential-flow pathways can result in distinct soil-moisture responses during the same rainfall event. In this study, we first characterized preferential-flow pathways using dye tracer experiments and then examined soil-moisture responses using observed soil-moisture data.

Dye tracer experiments were conducted on vegetated slopes near the soil-moisture monitoring sites to examine the preferential flow pathways (Fig. 1d). The slope angles were 35.8° at the woodland site and 38.2° at the shrubland site. An electric sprayer was used to spray a $4\,\mathrm{g\,L^{-1}}$ brilliant blue solution onto a $100\,\mathrm{cm} \times 100\,\mathrm{cm}$ plot (Fig. 4a and b). After spraying the solution, the plot was immediately covered with a rainproof cloth to minimize evaporation. After 24 h, a 5 cm-wide margin of soil was removed from the plot edges, and the core area was excavated to obtain 10 vertical and 5 horizontal profiles. Excavation grids were established at 0.1 m intervals in both the longitudinal and transverse directions (Fig. 4c and d). Profile images were captured with a digital camera at a fixed distance and in a parallel orientation, and subsequently processed using Adobe Photoshop (version 2021; Adobe Inc., USA) and Image-Pro Plus (version 6.0; Media Cybernetics, USA). The proportion of flow marked by the dye is:

$$\mathrm{SAR} = \frac{a_j}{A_j} \tag{1}$$

where SAR is the stained-area ratio for the soil profile, j is soil depth (cm), a is the number of stained pixels at depth j, and A is the total number of pixels along the image width at depth j.

The soil-moisture response index describes excess soil water in response to a given rainfall input:

$$R_C = \frac{R_{\max} - (R + R_0)}{R + R_0} \tag{2}$$

where R_C is the excess soil-water ratio in response to a given rainfall event, $R_{\max}$ is the maximum total soil-water storage during the rainfall episode (mm), R is the cumulative rainfall during the episode (mm), and R_0 is the initial total soil-water storage before the rainfall episode (mm). Positive or negative values of R_C indicate whether the increase in soil-water storage exceeds or falls below the rainfall input. In addition, R_C reflects the preferential-flow component aligned with slope orientation or gravity. As soil moisture typically lags rainfall, we follow the method proposed by Lu et al. (Lu et al., 2024), which defines rainfall episodes using soil depth and in situ saturated hydraulic conductivity measurements. Therefore, the R_C values under different $R + R_0$ conditions, together with the preferential-flow pathways, can reflect heterogeneity in soil-water movement in the woodland and shrubland.

3.4 Slope resistance to failure probability at given rainfall input

Hillslope resistance to failure at a given rainfall input depends on the topography and the physical, strength, and hydraulic properties of soil mass. A widely used combination of the infinite-slope stability model and a hydrological model yield an expression for the critical drainage area per unit contour length (Montgomery and Dietrich, 1994a):

$$a_{\mathrm{cr}} = \frac{zK\sin\theta\cos\theta}{R_{\mathrm{t}}} \times \left[\frac{C' + C_{\mathrm{r}}}{\rho_{\mathrm{w}} g z \cos^2\theta \tan\varphi} + \frac{\rho_{\mathrm{s}}}{\rho_{\mathrm{w}}}\left(1 - \frac{\tan\theta}{\tan\varphi}\right)\right] \tag{3}$$

where a_{cr} is the critical drainage area per unit contour length ($\mathrm{m^2\,m^{-1}}$), R_{t} is the triggering rainfall rate ($\mathrm{m\,d^{-1}}$), K is the saturated hydraulic conductivity ($\mathrm{m\,d^{-1}}$), θ is the slope angle (°), C' and C_{r} are the effective soil cohesion and the root-induced cohesion (kPa), ρ_{s} and ρ_{w} are the unit weights of soil and water ($\mathrm{KN\,m^{-3}}$), z is the landslide depth (m), and φ is the effective internal friction angle (°).

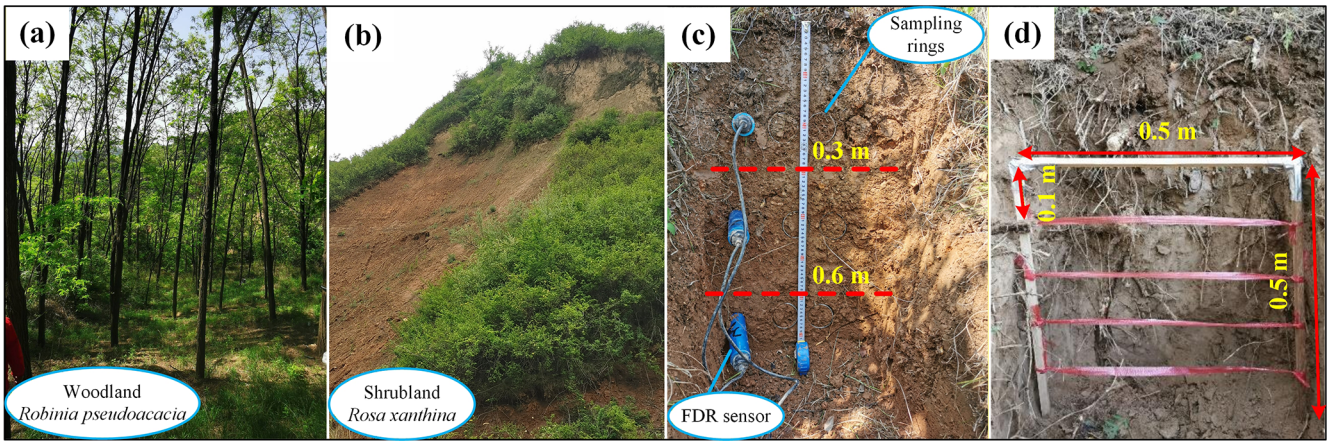

Figure 3. Soil moisture monitoring and soil and root sampling. **(a)** Open woodland dominated by *Robinia pseudoacacia*. **(b)** Close-structure shrubland dominated by *Rosa xanthina*. **(c)** Trench wall showing soil sampling and FDR sensor installation. **(d)** In situ root counting and sampling at 0.1 m depth intervals.

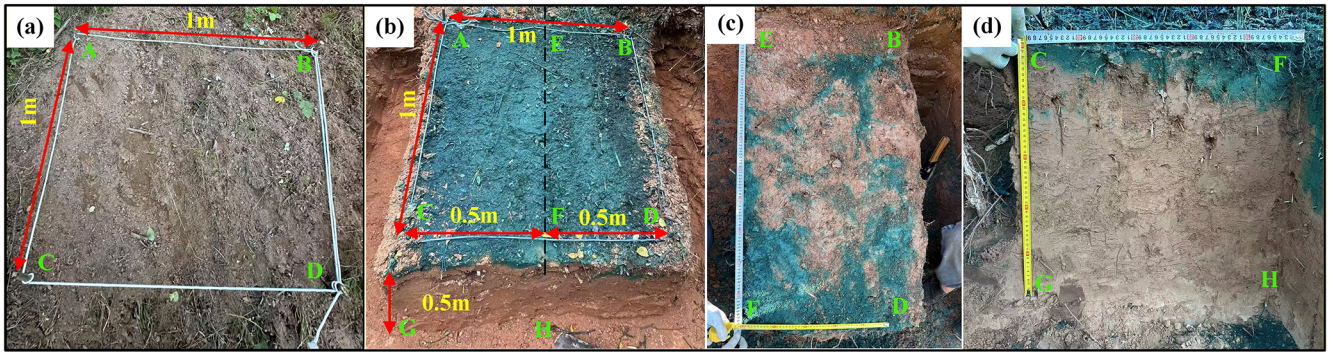

Figure 4. Dye tracer experiments and preferential flow pathways examination. **(a)** Experimental plot after vegetation removal. **(b)** Experimental plot after 24 h of brilliant blue solution spraying. **(c)** Dye-stained profile parallel to the slope surface. **(d)** Dye-stained profile along the gravity direction. Capital letters denote corresponding points shared across Fig. 4a–d.

The left-hand side of Eq. (3) represents the topographic condition of a given landslide or a site susceptible to slope failure (Montgomery et al., 2000). Moving R to the left-hand side yields the right-hand side of Eq. (4) in an integrated form involving only soil mass parameters:

$$a_{\mathrm{cr}} \times R_{\mathrm{t}} = \frac{K \tan\theta (C' + C_{\mathrm{r}})}{\rho_{\mathrm{w}} g \tan\varphi} + zK \sin\theta \cos\theta \frac{\rho_{\mathrm{s}}}{\rho_{\mathrm{w}}} \left(1 - \frac{\tan\theta}{\tan\varphi}\right) \quad (4)$$

The physical meaning of $a_{\mathrm{rc}} \times R_{\mathrm{t}}$ is that hillslope resistance to failure under site-specific topographic conditions and a given rainfall input strongly depends on soil physical properties. For the rain-induced loessal landslides in the study area, the strength and hydraulic properties of the landslide mass in woodland and shrubland may lead to different $a_{\mathrm{rc}} \times R_{\mathrm{t}}$ levels, so that landslide density (or number) differs between woodland and shrubland. Therefore, we focus on $a_{\mathrm{rc}} \times R_{\mathrm{t}}$ from the right-hand side of Eq. (4) to elucidate the initiation of loessal landslides in two forested land types.

4 Results

4.1 Landslides in the two lands

To compare the landslide point and areal densities between the two stands, we calculated landslide counts and areas and divided them by the total steep-terrain area in each stand. This approach excluded non-susceptible terrain from the analysis. The spatial distribution and morphology of landslides in woodland and shrubland exhibited clear patterns. Specifically, the statistical results showed that landslide point density in shrubland was 1.56 times that in woodland, whereas landslide areal density was only 0.48 times that in woodland (Fig. 5a and b). Furthermore, the average landslide width in shrubland was 1.49 times that in woodland. Generally, trees in woodlands have deep root systems that pro-

vide stronger anchoring and can mobilize deeper soil layers, thereby modifying the failure depth and geometry of shallow landslides (Schwarz et al., 2010; Masi et al., 2023; Dibiagio et al., 2024). The average landslide depth in woodland was 1.82 times that in shrubland, while the average lateral extent was 1.61 times that in shrubland. However, the average width of landslides in woodland was only 0.67 times that in shrubland. Overall, the total landslide volume in woodland was 1.16 times that in shrubland, indicating that landslides in woodland tend to be larger (Fig. 5c and d).

When landslides are considered alongside other landscape-dissection agents such as rills and gullies, their spatial locations depend on two controls. One is spatial competition between the slope-dependent term $S = \tan\theta$ ($\mathrm{m\,m^{-1}}$) and the area-dependent term A ($\mathrm{m^2\,m^{-1}}$); the other is exceedance of the A–S topographic threshold (Montgomery and Dietrich, 1994b). As highlighted in Sect. 3.4, variations in $a_{\mathrm{rc}} \times R_{\mathrm{t}}$ arise from the interplay of topography, failure depth, soil strength, plant root reinforcement, and hydraulic conductivity. To evaluate these controls on landslides, we compared the upslope contributing area (A) and slope gradient (S) between the two land types.

Field investigations reveal that most landslides in the study area occur in concave topographic positions. Statistical analysis indicates that, on average, woodland sites have a significantly larger upslope contributing area ($124\,\mathrm{m^2\,m^{-1}}$) and steeper slopes (48°) than shrubland sites. These values are consistent with expectations from the A–S threshold framework (Fig. 6a). Fitting regression lines to the bin-averaged dataset further demonstrates that landslides in woodland generally require either a larger upslope contributing area or a steeper slope gradient for initiation (Fig. 6b). The A–S relationship shows that, at similar slope gradients, landslides in woodland require larger upslope contributing areas than those in shrubland. This suggests that, compared with landslides in shrubland, those in woodland may require higher rainfall-intensity thresholds, steeper slopes, or both, for initiation. Consistent with this, shrubland shows a higher landslide point density than woodland (1.56 times; Fig. 5a).

4.2 Soil Hydrological properties

4.2.1 SWCC and HCF curves

Mean landslide depths in woodland and shrubland are 0.84 and 0.55 m, respectively (Fig. 5d). Soil-moisture monitoring and soil sampling were conducted at three depth intervals (0–30, 30–60, and 60–90 cm), as described in Sect. 3.2. Because observed landslide depths in woodland were mostly within 60–90 cm, this layer was taken as the representative sliding layer for woodland. Likewise, because observed landslide depths in shrubland were mostly within 30–60 cm, this layer was taken as the representative sliding layer for shrubland. Loess slopes generally remain unsaturated during natural rainfall infiltration and drainage (Lan et al., 2021; Wei et al., 2022). Therefore, we used the SWCC and HCF to analyze unsaturated hydro-mechanical differences between sliding-layer soils in woodland and shrubland.

Table 1 lists the sliding-layer soils parameters obtained through Hydrus-1D inversion. Based on these parameters, the SWCC and HCF were plotted for the woodland and shrubland sliding-layer soils (Fig. 7). The results indicate that the pore-size distribution parameter and saturated hydraulic conductivity are significantly higher for woodland soils than for shrubland soils. This contrast is evident in both drying and wetting processes. This suggests that the pore system in woodland soils is dominated by larger pores, which enhance water movement. This pore structure facilitates rainfall infiltration into the soil. In contrast, shrubland soils contain more micropores that retain more water. This is reflected in a 3.1 % higher residual water content in shrubland soils than in woodland soils. During the drying test, the air-entry pressures of woodland and shrubland soils are nearly identical. However, during the wetting process, the air-entry pressure in woodland soils is 0.05 kPa lower than in shrubland soils. This indicates that larger pores in woodland soils begin to drain and fill with air at lower matric suction. This promotes air-water exchange and moisture release, making it less likely for the soil to reach or maintain a high degree of saturation for extended periods. Therefore, under the same rainfall conditions, shrubland soils have weaker moisture-buffering capacity than woodland soils, making the soil more prone to becoming highly saturated. This reduces the effective stress and shear strength of shrubland soils, ultimately reducing slope stability.

During the drying and wetting processes, the difference in saturated water content in shrubland sliding-layer soil (0.101) is approximately 14.43 times that in woodland sliding-layer soil (0.007). This indicates that the pore structure in shrubland sliding-layer soil is less stable than in woodland sliding-layer soil. Under extreme drying-wetting conditions, some pores tend to collapse or rearrange, making it difficult for the soil to maintain its original pore configuration. The resulting changes in pore structure disrupt water flow paths in shrubland sliding-layer soil, reducing permeability, weakening water flow, and slowing drainage. These findings are consistent with the stronger hysteresis observed in the SWCC of shrubland sliding-layer soil compared with that of woodland sliding-layer soil (Fig. 7a and b). They further confirm that woodland sliding-layer soil has a greater capacity for moisture redistribution.

4.2.2 Dye tracer experiment

Dye-tracer experiments directly visualize the flow pathways of water infiltration in woodland and shrubland soils. Under the same applied water volume and infiltration area, the stained soil volume in woodland soils is markedly larger than that in shrubland soils. Three-dimensional visualizations reveal that stained pathways in woodland soils form

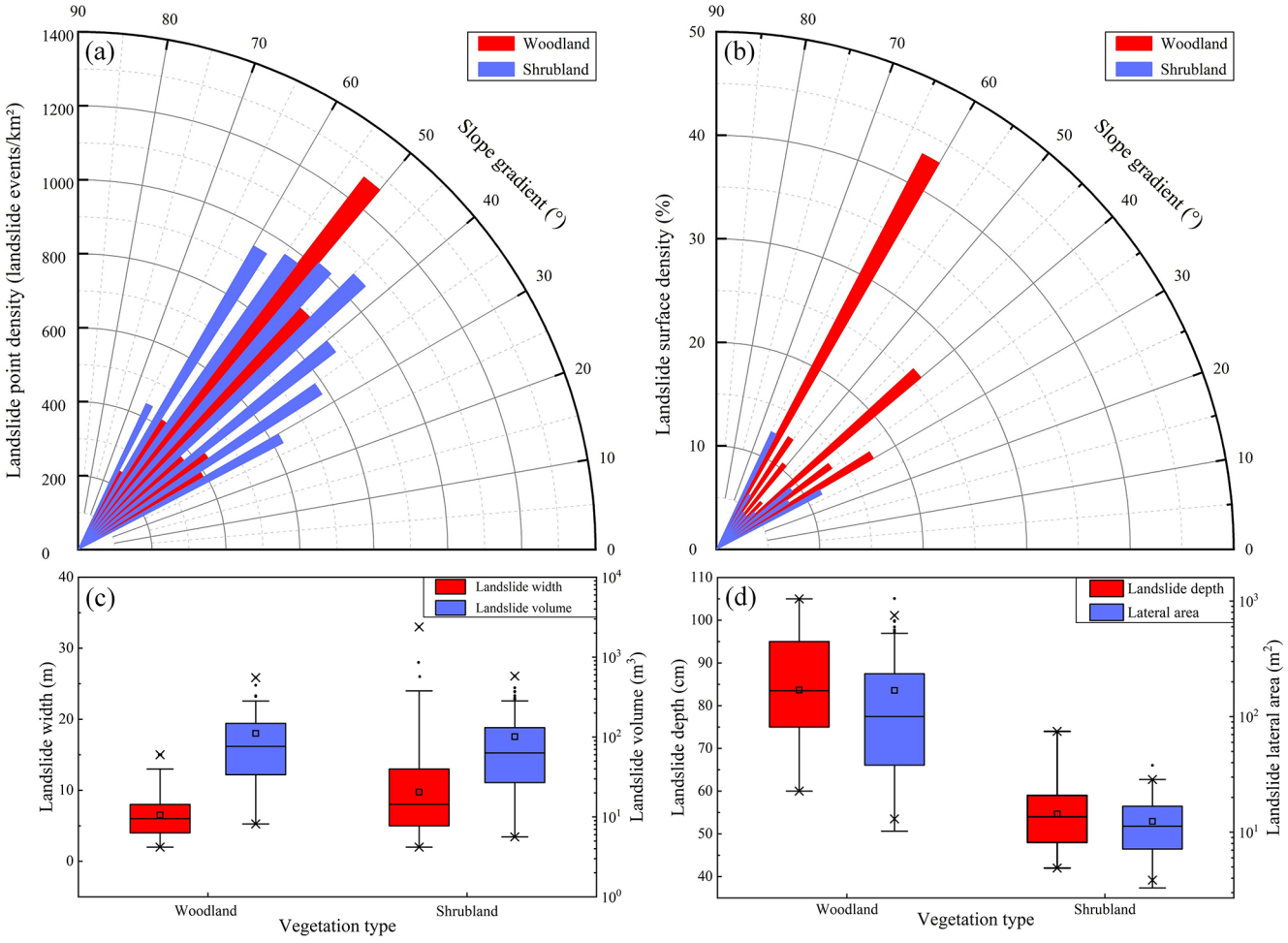

Figure 5. Landslide characteristics in woodland and shrubland. **(a)** Point density by slope-gradient class; **(b)** areal density by slope-gradient class; **(c)** landslide width and volume; and **(d)** landslide depth and lateral area. The three horizontal-lines of box show decreasing order of 75th quantile (Q_3), median (Q_2), and 25th quantile (Q_1). The box length is the interquartile range (IQR $= Q_3 - Q_1$). The small square is the average value. The cross symbols denote the 1st and 99th percentiles. The upper and lower limit of whiskers are $Q_3 + 1.5$ IQR and $Q_1 - 1.5$ IQR, respectively. The whiskers extend to the most extreme values within these limits; mild outliers are shown as black dots.

Table 1. Parameters describing the soil water characteristic curve (SWCC) and the hydraulic conductivity function (HCF) for the sliding-layer soils used in Hydrus 1D.

Parameters	Definition	Woodland	Shrubland
θ_s^d θ_s^w	Saturated water content	0.500 0.493	0.480 0.379
θ_r	Residual water content	0.055	0.086
n^d n^w	The pore size distribution parameter	1.58 1.69	2.19 1.88
a^d (KPa^{-1}) a^w (KPa^{-1})	The inverse of the air entry pressure head	5.461×10^{-3} 0.646	6.294×10^{-3} 0.596
K_s^d (cm s^{-1}) K_s^w (cm s^{-1})	Saturated hydraulic conductivity	2.3×10^{-5} 7.1×10^{-2}	5.4×10^{-6} 5.0×10^{-3}

Notes: Superscripts "d" and "w" denote the drying and wetting processes, respectively.

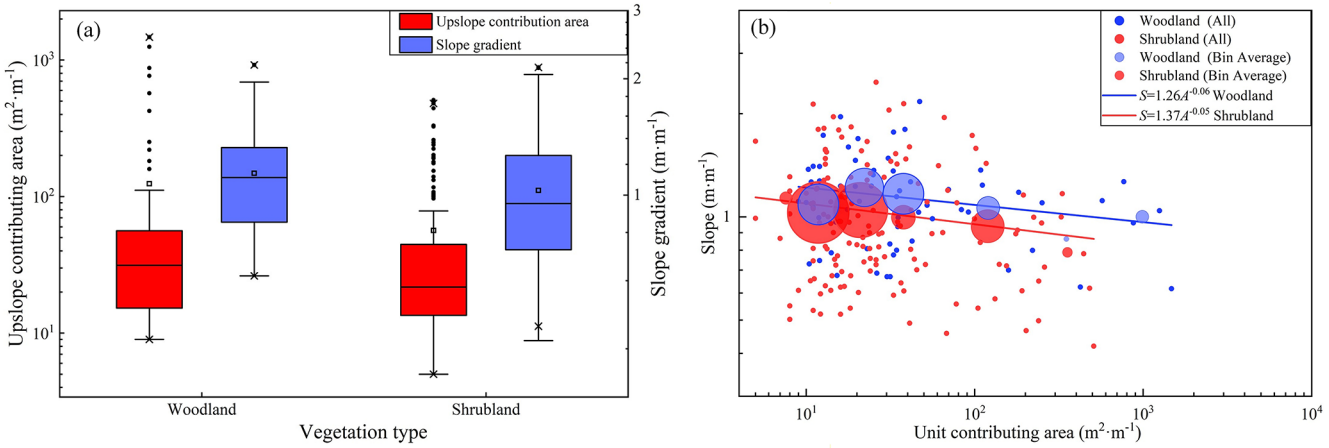

Figure 6. Upslope contributing area and slope gradient condition. **(a)** Upslope contributing area and mean slope as a function of slope aspect; **(b)** upslope contributing area vs. mean slope gradient above the landslide area. The definition of the boxplots is given in the caption of Fig. 5. Circles indicate mean slopes, with radius proportional to the number of landslides. A power-law regression is fitted to the bin-averaged data.

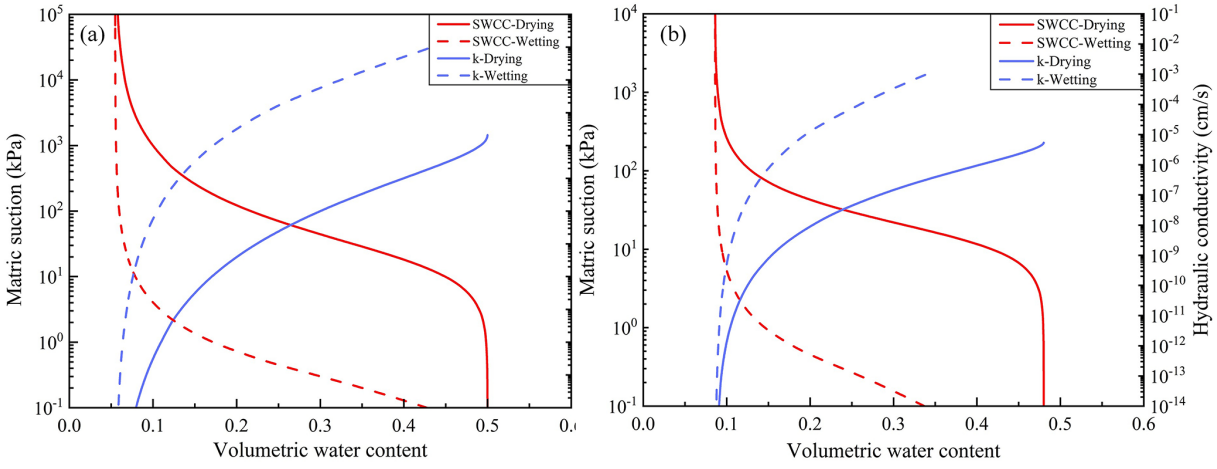

Figure 7. Differences in the hydromechanical properties of the sliding-layer soils. **(a)** SWCC for layer 3 of the woodland soil profile; **(b)** SWCC for layer 2 of the shrubland soil profile.

thick bands with numerous vertically continuous columnar channels (Fig. 8a). Hydraulic connectivity is high, and water infiltrates to greater depths. Stained bands in shrubland soils are shallow, and vertical, filament-like channels are nearly absent (Fig. 8b). In addition, the depth-dependent pattern of dye-stained area ratios in the shrubland profile further confirms that vertical infiltration is restricted to relatively shallow depths (Fig. 8d). Differences in the volume, depth, and morphology of the stained pathways indicate that infiltration in woodland soils no longer follows uniform matrix-flow conditions (Fig. 8a and c). This is also evident in the dye-stained areas of vertical profiles. Woodland profiles show large, continuous color patches, whereas shrubland profiles mainly show fragmented spots concentrated in shallow soil (Fig. 9). This pattern suggests that deeper shrubland soils are denser and have lower pore connectivity.

Overall, woodland soils more readily develop a stable, efficient vertical percolation system with greater infiltration depth and stronger connectivity. This promotes deep water storage and redistribution. In contrast, insufficient pore connectivity in shrubland soils causes water to remain in shallow layers, prolonging surface wetness and slowing pore-water pressure recovery. Under intense rainfall, this condition favors saturation buildup and thus increases the likelihood of landslide initiation. This flow pattern is consistent with the SWCC- and HCF-inferred differences in soil hydraulic behavior and provides direct, pathway-scale evidence of flow pathways, which cannot be resolved from the curve-derived hydraulic parameters alone.

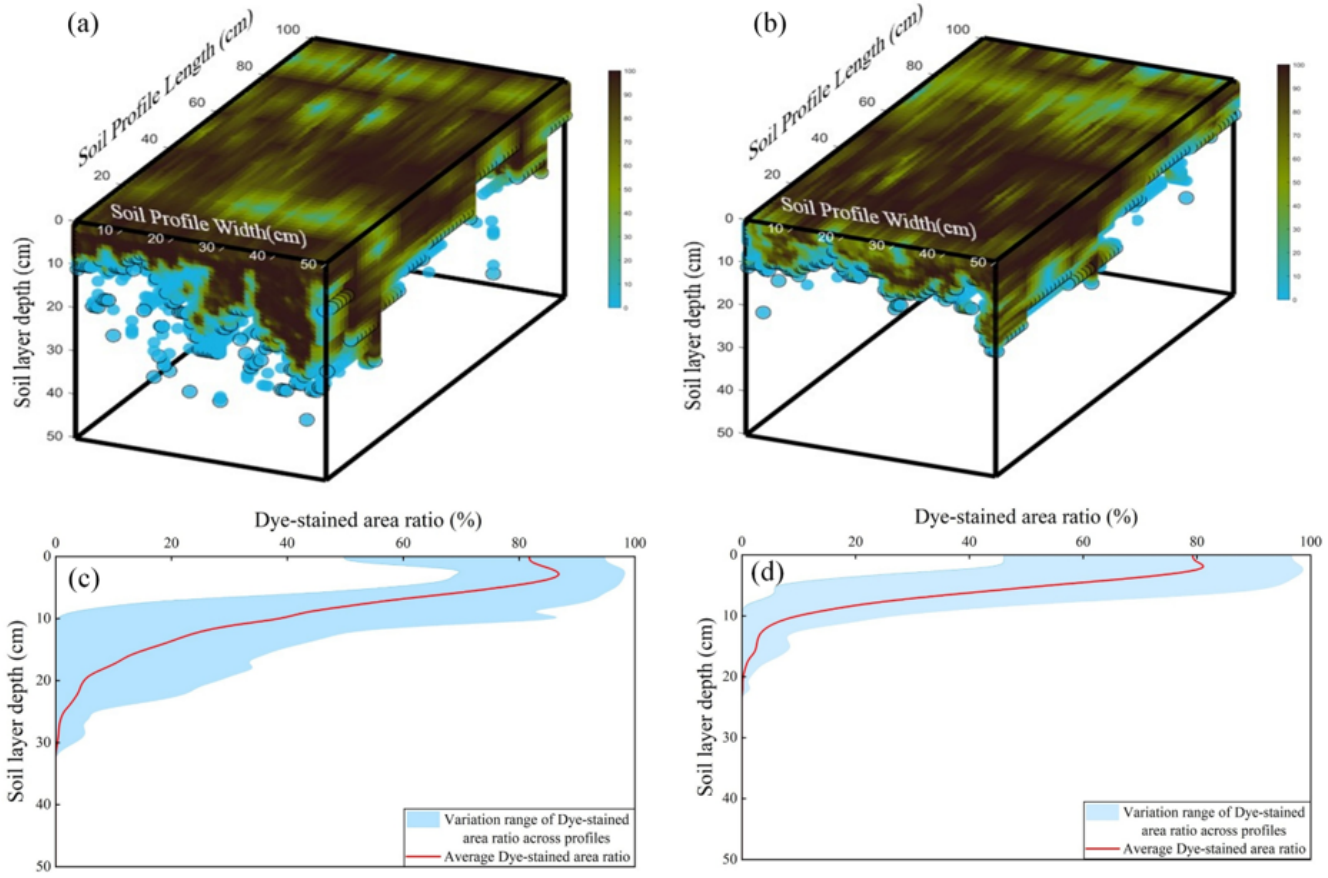

Figure 8. Morphological characteristics of dye-stained flow paths in woodland and shrubland soils. **(a)** Three-dimensional visualization of stained zones in woodland; **(b)** three-dimensional visualization of stained zones in shrubland; **(c)** dye-stained area ratio vs. soil depth in woodland; **(d)** dye-stained area ratio vs. soil depth in shrubland.

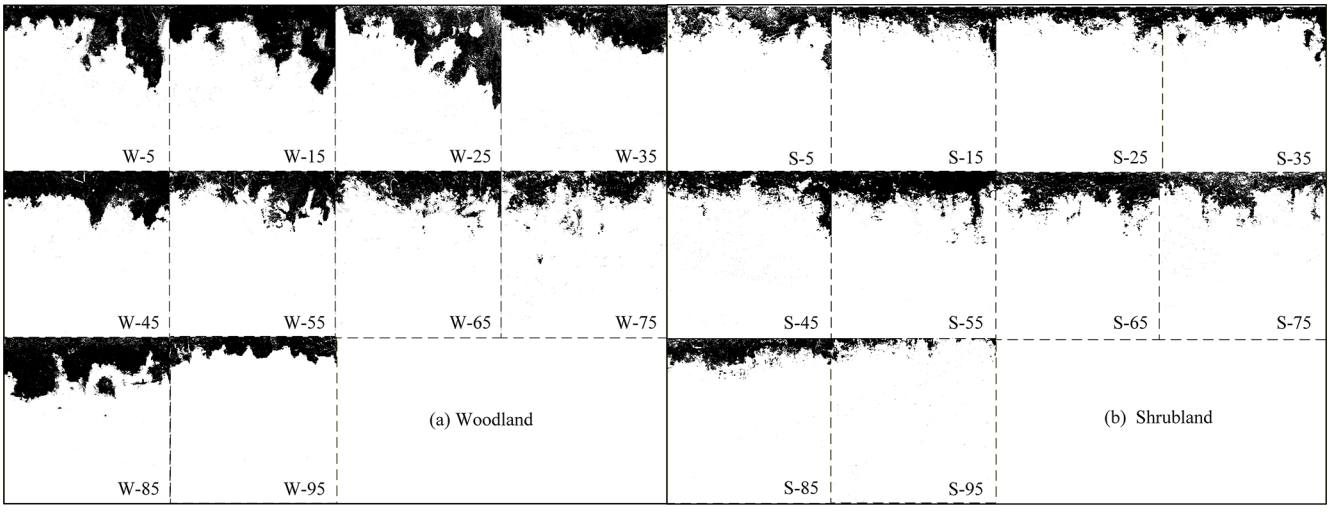

Figure 9. Schematic dye-stained vertical soil profiles at different hillslope positions. **(a)** Woodland profile; **(b)** shrubland profile. Numbers from 0 to 100 denote relative slope positions, with lower values indicating locations near the slope base.

4.3 Slope hydrological characteristics

To characterize how woodland and shrubland soils respond to rainfall, we group rainfall events into distinct episodes based on soil depth and in rain saturated hydraulic conductivity (Fig. 10a). Using these episodes as the basic analytical units, we then assess the intensity of slope-surface responses and the associated water distribution. This approach overcomes the limitations of using rainfall statistics alone. It explicitly addresses the slope's dynamic absorption-response behavior and shifts the focus from single-storm triggering to a more comprehensive assessment of cumulative rainfall-response lags.

From 22 May to 7 July 2023, volumetric water content indicates that shrubland soils beneath the sliding layer (layer 3) are insensitive to rainfall and show only small variations in water content (Fig. 10b). This is consistent with the findings in Sect. 4.2. In shrubland, most water remains near the surface, and infiltration capacity is low. To characterize the rainfall-soil-water coupling process, we introduce the index R_C, which quantifies how efficiently rainfall is converted into soil-water storage (Fig. 10c). A steeper slope in the regression of R_C versus soil water storage indicates a stronger soil-moisture response to rainfall.

In woodland, R_C values are generally positive, indicating that increases in soil-water content often exceed local rainfall input. Woodland soils have better-developed preferential flow paths than shrubland soils. This suggests that the observed excess arises because water infiltrating into upslope soils moves downslope as subsurface flow. This interpretation is consistent with the dye-tracer experiments. In woodland, foot-slope profiles show greater staining depths than upslope profiles (Fig. 8a). By contrast, early shallow saturation in shrubland diverts part of the rainfall input into overland flow, reducing conversion efficiency and yielding mostly negative R_C values. Overall, high R_C values in woodland reflect a strong hydrological response to rainfall and a greater capacity to buffer soil moisture. In shrubland, a pronounced response lag and low conversion efficiency lead to negative R_C values. These patterns are consistent with the earlier mechanism-based interpretation.

4.4 Effects of vegetation roots on hillslope stability

Root spatial distribution and mechanical properties differ markedly between woodland and shrubland soils (Fig. 11a–c). Field measurements indicate that maximum rooting depths in *Robinia pseudoacacia* and *Rosa xanthina* are close to their respective mean landslide depths, at 0.84 m in *Robinia pseudoacacia* and 0.54 m in *Rosa xanthina*. This consistency indicates a close relationship between root distribution and landslide depth. Compared with *Rosa xanthina*, roots in *Robinia pseudoacacia* mobilize greater root-induced cohesion at a given root diameter and exhibit a larger specific root area ratio (RAR). These roots therefore create a more extensive root-soil contact interface and form a mechanically stronger root-soil composite.

Table 2. Parameters describing the slope stability model.

Parameters	Definition	Woodland	Shrubland
ρ_s (kg m^{-3})	Dry soil density	1.37	1.41
θ (°)	Slope gradient	31.71–65.27	22.78–67.96
C' (kPa)	Effective soil cohesion	5.97	7.35
C_r (kPa)	Root-induced cohesion	18.59	10.36
φ (°)	Effective friction angle	18.67	14.50
z (m)	Landslide depth	0.84	0.54
K (mm h^{-1})	Hydraulic conductivity	2.10	0.94

Using the parameters in Table 2, we constructed a slope stability model to evaluate slope resistance to failure under specified topographic conditions and rainfall inputs. When root-induced cohesion is ignored, mean $a_{rc} \times R_t$ values in woodland and shrubland are similar, indicating that slope stability differs little between them. When root effects are included, slope stability increases markedly. In woodland, the $a_{rc} \times R_t$ value rises to 15.02, approximately 338 % higher than in shrubland (Fig. 11d). These results indicate that woodland roots contribute much more to slope stability than roots in shrubland. Woodland roots substantially increase the critical rainfall and topographic thresholds for landslide initiation and confirm the key role of roots in strengthening slopes and resisting landslide-triggering factors.

5 Discussion

Long-term vegetation restoration policies may result in the dominant soil erosion process shift from traditional wind and water erosion to landslides (Deng et al., 2022; Yang et al., 2024; Du et al., 2025; Liao et al., 2025). Ecological restoration forests not only increase surface cover, but the recovered vegetation extends their root systems into potential sliding layers, thereby substantially altering slope hydrological processes and mechanical properties, and playing an important role in landslide initiation (Zhao et al., 2022; Cai et al., 2024; Chen et al., 2024; Lann et al., 2024). In this context, our results highlight the hydro-mechanical heterogeneity across the *Robinia pseudoacacia*-dominated woodland and *Rosa xanthina*-dominated shrubland, and assessed its influence on landslide initation.

The results of SWCC and HCF agree well with the infiltration patterns observed in dye-tracer experiments. In woodland soils, continuous preferential flow channels promote rapid infiltration, substantial downward water migration, and a high capacity for water storage and drainage. Shrubland soils exhibit scattered preferential flow channels, shorter infiltration pathways, pronounced shallow saturation, and a weaker capacity for water redistribution. The stained area ratio and patch distribution further corroborate these differences. Woodland profiles display vertical and continuous

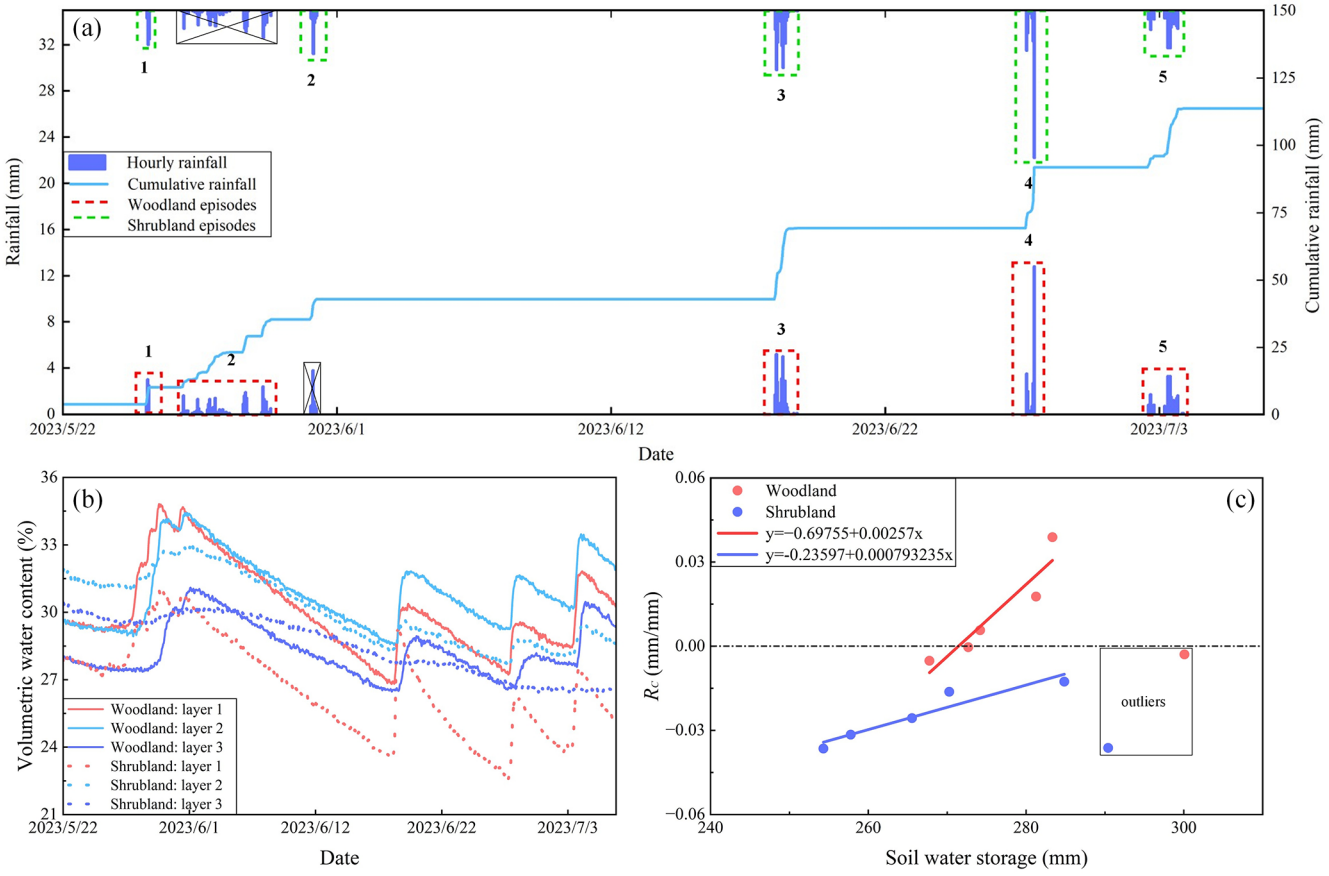

Figure 10. Analysis of rainfall, soil moisture, and their coupling from 22 May to 7 July 2023. **(a)** Classification of rainfall episodes by vegetation type; **(b)** temporal variation in volumetric soil water content for woodland and shrubland; **(c)** C coupling between rainfall input and soil-moisture response for woodland and shrubland.

stained bands with greater infiltration depths, whereas shrubland profiles show shallow staining. This comparison indicates that variations in root distribution and diameter modify soil pore structure and thereby affect infiltration (Guan et al., 2024; Lann et al., 2024). Woodland soil with coarse roots and higher porosity facilitate deeper infiltration, whereas shrubland soils with shallow root systems provide lower infiltration capacity (Souza et al., 2023; Xiao et al., 2024; Hu et al., 2025). Preferential flow may result in the excess soil water storage over the rainfall depth, and the results from monitoring multiple natural rainfall events between 20 May and 6 July 2023 further corroborate the assumption. In shrubland, soil moisture typically exhibits a delayed and attenuated response to rainfall. R_C values are consistently below zero, indicating low rainfall conversion efficiency. Most rainwater does not infiltrate but instead runs off once shallow soils saturate rapidly. In contrast, once rainfall over woodland slopes reaches a certain intensity, R_C values become positive. This pattern suggests that woodland slopes effectively intercept and infiltrate rainfall, sustain deeper water storage, and delay the development of saturation zones. This discrepancy is also evident in the critical $a_{rc} \times R_t$ values. The failure resistance on woodland slopes is higher than shrubland slopes, which may explain the contrasting distribution patterns observed in landslide number and size.

Vegetation-based slope protection has long been regarded as a key measure in traditional soil and water conservation, yet multidisciplinary studies have revealed its dual effects (Gyssels et al., 2005; Sidle and Bogaard, 2016; Lann et al., 2024). Some herbaceous plants with shallow root systems can promote rapid surface saturation during intense rainfall, thereby enhancing hillslope runoff and rill erosion (Gong et al., 2024). Certain fast-growing tree species with shallow root systems may provide only limited soil reinforcement and thus increase the risk of shallow landslides (Ghestem and Sidle, 2011; Lin et al., 2024). Moreover, excessively thick litter layers can impede infiltration during short-duration storms and accelerate runoff concentration (Zhou et al., 2018; Rajão et al., 2023). These observations indicate that vegetation-based measures are not universally effective for soil erosion control (Löbmann et al., 2020; Lann et al., 2024). Our results further support this understanding. Shallow landslide initia-

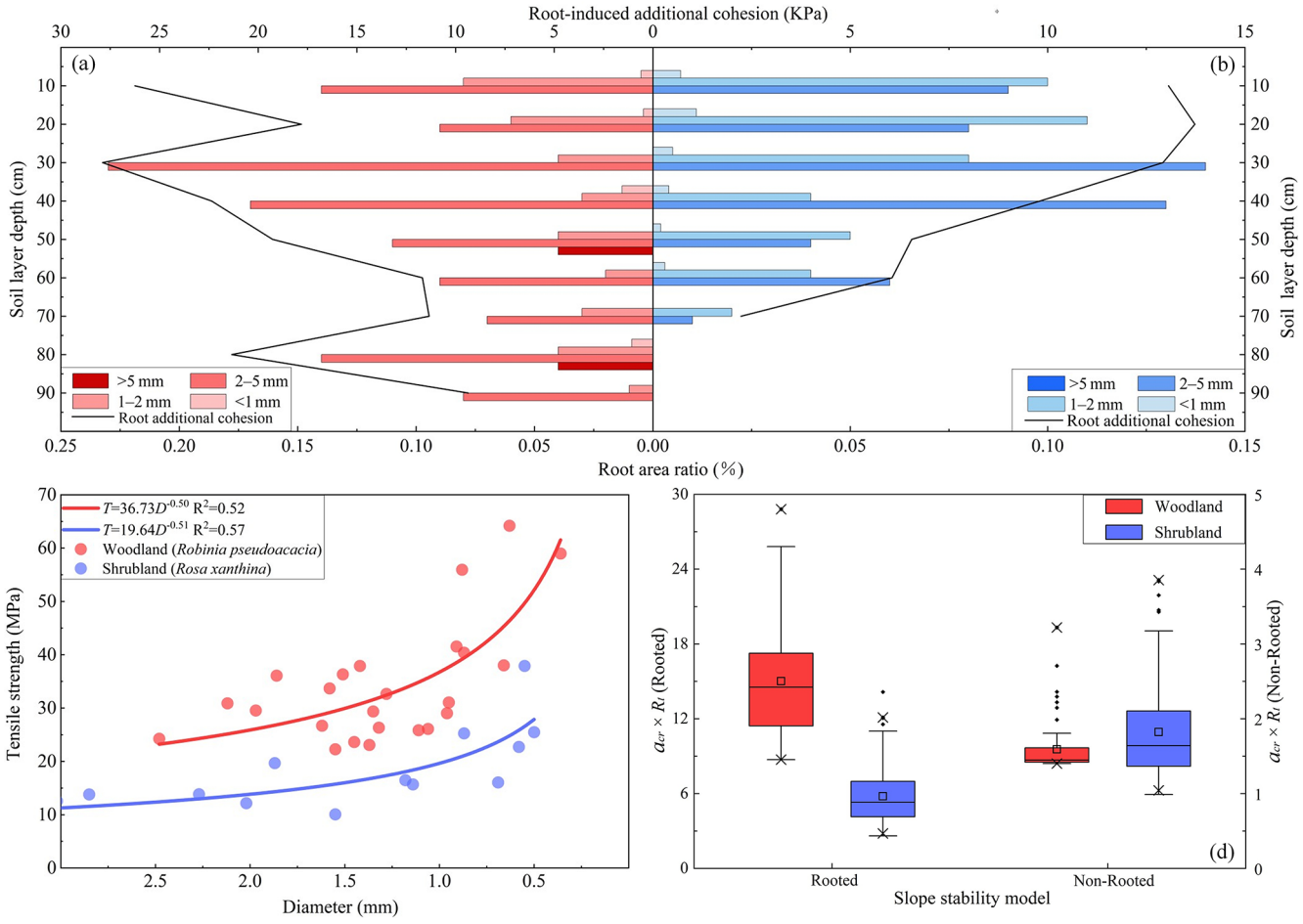

Figure 11. Mechanical indices of slope stability in woodland and shrubland. **(a)** Root area ratio and root-induced cohesion in woodland (*Robinia pseudoacacia*); **(b)** root area ratio and root-induced cohesion in shrubland (*Rosa xanthina*); **(c)** relationship between root tensile strength and diameter; **(d)** slope-stability models for woodland and shrubland. The definitions of the boxplots is given in the caption of Fig. 5.

tion depends not only on rainfall but also on vegetation type, which modifies coupled hydrological-mechanical processes on slopes. The deep root systems and stable preferential flow channels in woodland slopes may provide greater resilience against slope failure compared to shrubland slopes. This finding provides empirical evidence for forest-type allocation in ecologically sensitive areas. It also highlights the need for appropriate vegetation-type selection and matching in regional soil and water conservation.

6 Conclusions

Vegetation recovery on the Chinese Loess Plateau has altered the dominant soil erosion process from runoff-driven erosion to gravity-driven mass movements. Though previous studies have extensively investigated vegetation effects on soil erosion, the specific role of vegetation in landslide initiation remains poorly understood. In this study, we systematically examined landslide initiation processes in two contrasting vegetated landscapes: *Robinia pseudoacacia*-dominated woodlands and *Rosa xanthina*-dominated shrublands, focusing on hydro-mechanical heterogeneity. Following results can be drawn:

1. Landslides in woodland and shrubland exhibit obvious differences in initiation, depth and number. Shrubland has a higher density of small, shallow landslides, whereas woodland has fewer but deeper and larger failures. This contrast reflects a high-initiation-threshold and deep-seated-failure regime in woodland.

2. In shrubland, a loose, discontinuous pore system and pronounced hysteresis concentrate moisture in shallow layers, causing rapid shallow saturation and large rainfall losses. In woodland, stable preferential flow paths promote deeper and more efficient moisture migration, as reflected in higher soil water response index.

3. Woodland roots extend deeper and span a wider depth range than shrubland roots. Within the same depth

interval, root additional cohesion and RAR are also higher than those in shrubland. These patterns indicate stronger root-network reinforcement in woodland soils and lower susceptibility to shallow landslides than in shrubland. Therefore, the sediment production from landslide erosion may differ in various forest types, which has been rarely addressed and deserves further study in future.

Data availability. The corresponding author, Prof. Chao Ma, is willing to share the raw/processed data upon reasonable request.

Author contributions. Prof. Ma conceived the study based on his expertise in shallow landslides and unsaturated soil mechanics, and proposed the concept of hydrological and hydromechanical coupling for analyzing vegetation-related slope instability. Under the guidance of Prof. Ma. Ruijie Yang conducted soil hydrology experiments and drafted the manuscript. Xi Yang and Xinying Wang assisted with field investigations. Yan Zang and Liqun Lyu contributed research progress on shallow landslides and vegetation–slope interactions in the study area.

Competing interests. The contact author has declared that none of the authors has any competing interests.

Disclaimer. Publisher's note: Copernicus Publications remains neutral with regard to jurisdictional claims made in the text, published maps, institutional affiliations, or any other geographical representation in this paper. The authors bear the ultimate responsibility for providing appropriate place names. Views expressed in the text are those of the authors and do not necessarily reflect the views of the publisher.

Acknowledgements. The authors extend their gratitude to personnel at the Jixian National Ecosystem Research Station of Shanxi Province, Beijing Forestry University, for their help during field investigations.

Financial support. This research has been supported by the State Key Program of Natural Science of China (grant no. 42130701), and the Natural Science Foundation of China (grant no. 42177309).

Review statement. This paper was edited by Roberto Greco and reviewed by two anonymous referees.

References

An, J., Gao, G., Yuan, C., Pinos, J., and Fu, B.: Inter- and intra-event rainfall partitioning dynamics of two typical xerophytic shrubs in the Loess Plateau of China, Hydrol. Earth Syst. Sci., 26, 3885–3900, https://doi.org/10.5194/hess-26-3885-2022, 2022.

Bachmair, S., Weiler, M., and Troch, P. A.: Intercomparing hillslope hydrological dynamics: spatio-temporal variability and vegetation cover effects, Water Resour. Res., 48, W5537, https://doi.org/10.1029/2011WR011196, 2012.

Bai, R., Wang, X., Li, J., Yang, F., Shangguan, Z., and Deng, L.: The impact of vegetation reconstruction on soil erosion in the loess plateau, J. Environ. Manage., 363, 121382, https://doi.org/10.1016/j.jenvman.2024.121382, 2024.

Borrelli, P., Robinson, D. A., Panagos, P., Lugato, E., Yang, J. E., Alewell, C., Wuepper, D., Montanarella, L., and Ballabio, C.: Land use and climate change impacts on global soil erosion by water (2015–2070), P. Natl. Acad. Sci. USA, 117, 21994–22001, https://doi.org/10.1073/pnas.2001403117, 2020.

Cai, L., Wang, F., Lin, Y., Long, Q., Zhao, Y., Han, J., Ge, W., and Chen, H.: Changes in preferential flow caused by root effects in black locust plantations of different stand ages in the semi-arid region of the loess plateau, J. Hydrol., 634, 131086, https://doi.org/10.1016/j.jhydrol.2024.131086, 2024.

Chen, M., Yang, X., Zhang, X., Bai, Y., Shao, M., Wei, X., Jia, Y., Wang, Y., Jia, X., Zhu, Y., Zhang, Q., Zhu, X., and Li, T.: Response of soil water to long-term revegetation, topography, and precipitation on the chinese loess plateau, Catena, 236, 107711, https://doi.org/10.1016/j.catena.2023.107711, 2024.

Deng, J., Ma, C., and Zhang, Y.: Shallow landslide characteristics and its response to vegetation by example of july 2013, extreme rainstorm, central loess plateau, china, B. Eng. Geol. Environ., 81, 100, https://doi.org/10.1007/s10064-022-02606-1, 2022.

Dibiagio, A., Capobianco, V., Oen, A., and Tallaksen, L. M.: State-of-the-art: parametrization of hydrological and mechanical reinforcement effects of vegetation in slope stability models for shallow landslides, Landslides, 21, 2417–2446, https://doi.org/10.1007/s10346-024-02300-1, 2024.

Du, P., Chen, Y., Zhao, Y., Qu, L., Liu, H., Liu, Z., Xu, J., and Tian, X.: Formation process and depositional characteristics of mudballs in the loess plateau during extreme rainstorms: dual-threshold constraints on material sources and dynamic conditions, J. Environ. Manage., 391, 126590, https://doi.org/10.1016/j.jenvman.2025.126590, 2025.

Fan, L., Lehmann, P., Zheng, C., and Or, D.: Rainfall intensity temporal patterns affect shallow landslide triggering and hazard evolution, Geophys. Res. Lett., 47, e2019GL085994, https://doi.org/10.1029/2019GL085994, 2020.

Feng, X., Fu, B., Piao, S., Wang, S., Ciais, P., Zeng, Z., Lü, Y., Zeng, Y., Li, Y., Jiang, X., and Wu, B.: Revegetation in china's loess plateau is approaching sustainable water resource limits, Nat. Clim. Change, 6, 1019–1022, https://doi.org/10.1038/nclimate3092, 2016.

Franklin, S. M., Kravchenko, A. N., Vargas, R., Vasilas, B., Fuhrmann, J. J., and Jin, Y.: The unexplored role of preferential flow in soil carbon dynamics, Soil Biol. Biochem., 161, 108398, https://doi.org/10.1016/j.soilbio.2021.108398, 2021.

Fu, B., Wang, S., Liu, Y., Liu, J., Liang, W., and Miao, C.: Hydrogeomorphic ecosystem responses to natural and anthropogenic changes in the loess plateau of china, Annu. Rev. Earth Pl. Sc., 45, 223–243, https://doi.org/10.1146/annurev-earth-063016-020552, 2016.

Ghestem, M. and Sidle, R.: The influence of plant root systems on subsurface flow: implications for slope stability, Bioscience, 61, 869–879, https://doi.org/10.1525/bio.2011.61.11.6, 2011.

Gong, C., Ni, D., Liu, Y., Li, Y., Huang, Q., Tian, Y., and Zhang, H.: Herbaceous vegetation in slope stabilization: a comparative review of mechanisms, advantages, and practical applications, Sustainability-Basel, 16, 7620, https://doi.org/10.3390/su16177620, 2024.

Gu, C., Mu, X., Gao, P., Zhao, G., Sun, W., Tatarko, J., and Tan, X.: Influence of vegetation restoration on soil physical properties in the loess plateau, china, J. Soil. Sediment., 19, 716–728, https://doi.org/10.1007/s11368-018-2083-3, 2019.

Guan, N., Bi, H., Song, Y., Lu, S., Lin, D., and Han, J.: Vegetation restoration is affecting the characteristics and patterns of infiltration in the loess plateau, Catena, 243, 108190, https://doi.org/10.1016/j.catena.2024.108190, 2024.

Gyssels, G., Poesen, J., Bochet, E., and Li, Y.: Impact of plant roots on the resistance of soils to erosion by water: a review, Prog. Phys. Geog., 29, 189–217, https://doi.org/10.1191/0309133305pp443ra, 2005.

Hao, M., Jin, Z., Luo, D., Cao, G., Jiang, C., Han, H., Yang, S., and Zhang, J.: Rainstorm erosion difference and topographical changes induced by heavy rainfall between afforestation and grassland restoration catchments on the chinese loess plateau, Geomorphology, 457, 109243, https://doi.org/10.1016/j.geomorph.2024.109243, 2024.

Hu, J., Ren, Y., Tang, M., Zhang, Z., Yang, K., Zhen, Q., and Han, F.: Effects of vegetation restoration on infiltration patterns and preferential flow in semi-arid areas with shallowly buried soft bedrock (pisha sandstone) in china, J. Hydrol., 661, 133546, https://doi.org/10.1016/j.jhydrol.2025.133546, 2025.

Lan, H., Zhao, X., Macciotta, R., Peng, J., Li, L., Wu, Y., Zhu, Y., Liu, X., Zhang, N., and Liu, S.: The cyclic expansion and contraction characteristics of a loess slope and implications for slope stability., Sci. Rep., 11, 2250, https://doi.org/10.1038/s41598-021-81821-4, 2021.

Lann, T., Bao, H., Lan, H., Zheng, H., Yan, C., and Peng, J.: Hydro-mechanical effects of vegetation on slope stability: a review, Sci. Total Environ., 926, 171691, https://doi.org/10.1016/j.scitotenv.2024.171691, 2024.

Laycock, W. A.: Distribution of roots and rhizomes in different soil types in the pine barrens of New Jersey, U.S. Geological Survey Professional Paper 563-C, Washington, https://doi.org/10.3133/pp563C, 1967.

Li, F., Song, X., Tang, C., Liu, C., Yu, J., and Zhang, W.: Tracing infiltration and recharge using stable isotope in taihang mt., North china, Environ. Geol., 53, 687–696, https://doi.org/10.1007/s00254-007-0683-0, 2007.

Li, J., Cui, P., and Yin, Y.: Field observation and micromechanism of roots-induced preferential flow by infiltration experiment and phase-field method, J. Hydrol., 623, 129756, https://doi.org/10.1016/j.jhydrol.2023.129756, 2023.

Li, S., Zheng, C., Lu, T., Zhou, K., Gu, Y., Wang, B., and Lu, Y.: Characteristics and influencing factors of loess terraces' preferential flow under different typical vegetation cover, Plant Soil, 515, 2135–2153, https://doi.org/10.1007/s11104-025-07710-1, 2025.

Liang, H., Li, Y., An, X., Liu, J., Pan, N., and Li, Z.: Soil moisture dynamics and its temporal stability under different-aged caragana korshinskii shrubs in the loess hilly region of china, Water-Sui, 15, 2334, https://doi.org/10.3390/w15132334, 2023.

Liao, J., Wang, J., Jiao, J., Yan, Z., Li, J., Zhang, Z., Li, M., Xu, Q., Jiang, X., Zhao, W., Ling, Q., Sheng, H., Chen, Y., and Wu, T.: Rusle tends to overestimate soil erosion in revegetated conditions: evidence from long-term runoff plots monitoring on china's loess plateau, Catena, 258, 109285, https://doi.org/10.1016/j.catena.2025.109285, 2025.

Lin, Y., Jian, W., Wu, Y., Zhu, Z., Wang, H., Dou, H., and Lai, Z.: Effect of tree roots on heavy rainfall-induced shallow landslides, Geomat. Nat. Haz. Risk, 15, 2360002, https://doi.org/10.1080/19475705.2024.2360002, 2024.

Liu, X., Feng, T., Zhang, Y., Liu, Y., and Wang, P.: Vegetation restoration affects soil hydrological processes in typical natural and planted forests on the loess plateau, J. Hydrol., 650, 132465, https://doi.org/10.1016/j.jhydrol.2024.132465, 2025.

Löbmann, M. T., Geitner, C., Wellstein, C., and Zerbe, S.: The influence of herbaceous vegetation on slope stability – a review, Earth-Sci. Rev., 209, 103328, https://doi.org/10.1016/j.earscirev.2020.103328, 2020.

L Lu, N. and Godt, J. W. (Eds.): Hillslope hydrology and stability, Cambridge University Press, Cambridge, UK, ISBN 10 1107021065, 2013.

Lu, N., Calderon, A. R. A., Wayllace, A., Lovekin, J., and Crandall, A.: Suction stress–based rainfall intensity–duration method for slope instability prediction, J. Geotech. Geoenviron., 150, 4024069, https://doi.org/10.1061/JGGEFK.GTENG-12597, 2024.

Masi, E. B., Tofani, V., Rossi, G., Cuomo, S., Wu, W., Salciarini, D., Caporali, E., and Catani, F.: Effects of roots cohesion on regional distributed slope stability modelling, Catena, 222, 106853, https://doi.org/10.1016/j.catena.2022.106853, 2023.

Montgomery, D. R. and Dietrich, W. E.: A physically based model for the topographic control on shallow landsliding, Water Resour. Res., 30, 1153–1171, https://doi.org/10.1029/93WR02979, 1994a.

Montgomery, D. R. and Dietrich, W. E.: Landscape dissection and drainage area-slope thresholds, in: Process Models and Theoretical Geomorphology, John Wiley & Sons, Chichester, 221–246, ISBN 10 0471941042, 1994b.

Montgomery, D. R., Schmidt, K. M., Greenberg, H. M., and Dietrich, W. E.: Forest clearing and regional landsliding, Geology, 28, 311–314, https://doi.org/10.1130/0091-7613(2000)28<311:FCARL>2.0.CO;2, 2000.

Nimmo, J. R., Perkins, K. S., Schmidt, K. M., Miller, D. M., Stock, J. D., and Singha, K.: Hydrologic characterization of desert soils with varying degrees of pedogenesis: 1. Field experiments evaluating plant-relevant soil water behavior, Vadose Zone J., 8, 480–495, https://doi.org/10.2136/vzj2008.0052, 2009.

Niu, F., Pan, C., and Cui, Y.: Experimental investigation to the effect of different land-use on rainfall infiltration runoff patterns and preferential flow distribution in the loess area of western shanxi province, Acta Ecologica Sinica, 43, 4144–4166, https://doi.org/10.5846/stxb202204130989, 2023.

Rajão, P., Berg, M., Cornelissen, J., and Dias, A.: The effects of leaf traits on litter rainfall interception with consequences for runoff and soil conservation, J. Ecol., 111, 2662–2675, https://doi.org/10.1111/1365-2745.14203, 2023.

Schwarz, M., Preti, F., Giadrossich, F., Lehmann, P., and Or, D.: Quantifying the role of vegetation in slope stability: a case study in tuscany (italy), Ecol. Eng., 36, 285–291, https://doi.org/10.1016/j.ecoleng.2009.06.014, 2010.

Sidle, R. C. and Bogaard, T. A.: Dynamic earth system and ecological controls of rainfall-initiated landslides, Earth-Sci. Rev., 159, 275–291, https://doi.org/10.1016/j.earscirev.2016.05.013, 2016.

Souza, L. F. T., Hirmas, D. R., Sullivan, P. L., Reuman, D. C., Kirk, M. F., Li, L., Ajami, H., Wen, H., Sarto, M. V. M., Loecke, T. D., Rudick, A. K., Rice, C. W., and Billings, S. A.: Root distributions, precipitation, and soil structure converge to govern soil organic carbon depth distributions, Geoderma, 437, 116569, https://doi.org/10.1016/j.geoderma.2023.116569, 2023.

Tang, B., Jiao, J., Zhang, Y., Chen, Y., Wang, N., and Bai, L.: The magnitude of soil erosion on hillslopes with different land use patterns under an extreme rainstorm on the northern loess plateau, china, Soil Till. Res., 204, 104716, https://doi.org/10.1016/j.still.2020.104716, 2020.

Tang, P., Zhang, J., Li, Y., Wei, G., Hu, Y., and Zhao, J.: Effects of extreme rainfall on the morphological characteristics and spatialdistribution of shallow landslides under different land use patterns in the loessregion of western shanxi province, northern china, Journal of Beijing Forestry University, 45, 109–117, https://doi.org/10.12171/j.1000-1522.20230070, 2023.

Wang, N. and Zhang, T.: Soil pore structure and its research methods: a review, Soil Water Res., 19, 1–24, https://doi.org/10.17221/64/2023-SWR, 2024.

Wang, R., Dong, Z., Zhou, Z., and Wang, P.: Temporal variation in preferential water flow during natural vegetation restoration on abandoned farmland in the loess plateau of china, Land, 8, 186, https://doi.org/10.3390/land8120186, 2019.

Wang, R., Dong, Z., Zhou, Z., Wang, N., Xue, Z., and Cao, L.: Effect of vegetation patchiness on the subsurface water distribution in abandoned farmland of the loess plateau, china, Sci. Total Environ., 746, 141416, https://doi.org/10.1016/j.scitotenv.2020.141416, 2020.

Wang, X., Ma, C., Lyu, L., and Zhang, Y.: Erosion characteristics of shallow landslides undervarious land-use conditions: an example of the caijiachuan landslide, Arid Zone Research, 41, 697–705, https://doi.org/10.13866/j.azr.2024.04.15, 2024.

Wang, Y., Dong, G., Qu, L., Wu, Z., Zhao, F., and Shao, C.: Ecosystem functioning of the loess plateau in china from vegetation restoration relied largely on climate, Forests, 14, 27, https://doi.org/10.3390/f14010027, 2022.

Wei, Y. Z., Yao, Z. H., Chong, X. L., Zhang, J. H., and Zhang, J.: Microstructure of unsaturated loess and its influence on strength characteristics, Sci. Rep., 12, 1502, https://doi.org/10.1038/s41598-022-05464-9, 2022.

Wen, S., Shao, M., and Wang, J.: Earthworm burrowing activity and its effects on soil hydraulic properties under different soil moisture conditions from the loess plateau, china, Sustainability-Basel, 12, 9303, https://doi.org/10.3390/su12219303, 2020.

Xiao, T., Li, P., Fei, W., and Wang, J.: Effects of vegetation roots on the structure and hydraulic properties of soils: a perspective review, Sci. Total Environ., 906, 167524, https://doi.org/10.1016/j.scitotenv.2023.167524, 2024.

Yamase, K., Ikeno, H., Hotta, N., Imawaka, M., Ohashi, M., Tanikawa, T., Todo, C., Dannoura, M., and Hirano, Y.: Effect of sprouting and corresponding root distribution of the shrub species eurya japonica on slope stability, Catena, 238, 107869, https://doi.org/10.1016/j.catena.2024.107869, 2024.

Yan, X., Nunes, J. P., Sun, J., Tang, D., Wen, Y., and Li, Z.: Restored vegetation dominates the decrease in surface and subsurface runoff on the loess plateau, J. Hydrol., 640, 131730, https://doi.org/10.1016/j.jhydrol.2024.131730, 2024.

Yang, B., Jiao, J., Ma, X., Zhao, W., Ling, Q., Zhang, X., Han, J., Du, P., Chen, Y., and Chen, H.: Distribution and formation of soil balls under heavy rainstorm conditions in the northern loess plateau, J. Hydrol., 625, 130103, https://doi.org/10.1016/j.jhydrol.2023.130103, 2023.

Yang, B., Ma, X., Jiao, J., Zhao, W., Ling, Q., Li, J., and Zhang, X.: Magnitude and hotspots of soil erosion types during heavy rainstorm events on the loess plateau: implications for watershed management, Catena, 246, 108365, https://doi.org/10.1016/j.catena.2024.108365, 2024.

Zhang, S., Liu, Y., Yang, M., Tian, P., Mu, X., and Zhao, G.: Impact of vegetation restoration on preferential flow and soil infiltration capacity in the hilly region of the loess plateau, Journal of Hydrology: Regional Studies, 59, 102333, https://doi.org/10.1016/j.ejrh.2025.102333, 2025.

Zhang, Y., Tang, Z., Zhang, J., Zhang, Z., and Zhang, M.: Visualizing preferential flow paths using dye tracer and species diversity theory methods to explore their correlation to soil properties with random forest algorithm, J. Hydrol., 638, 131570, https://doi.org/10.1016/j.jhydrol.2024.131570, 2024.

Zhao, M., Li, D., Huang, Y., Deng, Y., Yang, G., Lei, T., and Huang, Y.: Soil matrix infiltration characteristics in differently aged eucalyptus plantations in a southern subtropical area in china, Catena, 217, 106490, https://doi.org/10.1016/j.catena.2022.106490, 2022.

Zhou, Q., Zhou, X., Luo, Y., and Cai, M.: The effects of litter layer and topsoil on surface runoff during simulated rainfall in guizhou province, china: a plot scale case study, Water-Sui, 10, 915, https://doi.org/10.3390/w10070915, 2018.